# Inner Coordination Sphere Control of Metal−Metal Superexchange in Ruthenium Dimers

**Ali R. Rezvani,[†] Corinne Bensimon,[†] Benoit Cromp,[‡] Christian Reber,[‡] J. E. Greedan,[§] Veniamin V. Kondratiev,[||] and Robert J. Crutchley*,[†]**

Ottawa-Carleton Chemistry Institute, Carleton University, 1125 Colonel By Drive, Ottawa, Ontario, Canada K1S 5B6, Brockhouse Institute for Materials Research, McMaster University, Hamilton, Ontario, Canada L8S 4M1, Department of Chemistry, University of Montreal, Montreal, Quebec, Canada H3C 3J7, and St. Petersburg University, Universitekaja nab. 7-9, St. Petersburg 199034, Russia

*Received January 8, 1997*[⊗]

The dinuclear Ru(III) complexes *trans*-[{$(NH_3)_4$Ru(py)}$_2$($\mu$-L)][$PF_6$]$_4$, where py represents pyridine and L represents 1,4-dicyanamidobenzene dianion (dicyd$^{2-}$) derivatives dicyd$^{2-}$ (**1**), $Me_2$dicyd$^{2-}$ (**2**), $Cl_2$dicyd$^{2-}$ (**3**), and $Cl_4$dicyd$^{2-}$ (**4**), have been prepared and characterized by electronic absorption spectroscopy and cyclic voltammetry. A crystal structure of the complex *trans*-[{$(NH_3)_4$Ru(py)}$_2$($\mu$-dicyd)][$PF_6$]$_4$·$^1/_2H_2O$ showed the dicyd$^{2-}$ ligand to be approximately planar with the cyanamido groups in a *syn* configuration. Crystal structure data are space group $P2_1$, with $a$, $b$, and $c$ = 7.826(3), 20.455(7), and 14.428(5) Å, respectively, $\beta$ = 95.76 (3)°, $V$ = 2296.7(14) Å$^3$, and $Z$ = 2. The structure was refined by using 3292 reflections with $I > 2.5\sigma(I)$ to an $R$ factor of 0.069. Solid state magnetic susceptibility measurements of the Ru(III)−Ru(III) dimers showed diamagnetic behavior at room temperature, and this is suggested to be due to strong antiferromagnetic superexchange via the HOMO of the dicyd$^{2-}$ ligand. The bridging ligand dependence of metal−metal coupling in the Ru(III)−Ru(II) complexes of **1**, **2**, **3**, and **4** in acetonitrile solution was demonstrated by the trend in comproportionation constants, $1.5 \times 10^6$, $5.7 \times 10^6$, $1.4 \times 10^4$, and $1.1 \times 10^3$, respectively. In addition, comparison to the analogous pentaammineruthenium dimers showed that the magnitude of metal−metal superexchange could be controlled by the nature of the spectator ligand. Spectroelectrochemical methods were used to acquire the absorption spectra of the mixed-valence complexes, and the intervalence band properties were modeled with PKS theory. Metal−metal coupling in the Ru(III)−Ru(II) complexes of **1**, **2**, **3**, and **4** was analyzed by using Hush and CNS theories.

## Introduction

Two successful examples of magnetic and electronic materials based on coordination chemistry are the room temperature molecular magnet V(TCNE)$_x$·$y$($CH_2Cl_2$) where TCNE is tetracyanoethane[1] and the molecular metal [Cu(DCNQI)$_2$]$_n$ where DCNQI is *N*,*N*′-dicyanoquinodiimine.[2] Research into novel magnetic materials has been largely supported by the extensive body of knowledge concerning the mechanism and expression of magnetic exchange phenomena in polynuclear complexes.[3] In the quest for conducting coordination polymers, however, design criteria must be based on the rather limited knowledge gained through the study of mixed-valence complexes.[4] The limit to the knowledge available arises because the vast majority of mixed-valence systems (typically Ru(III,II) dimers) studied to date incorporate $\pi$-acceptor bridging ligands, with very little work having been done on dinuclear complexes bridged by $\pi$-donor ligands. Thus, information on electron transfer superexchange abounds, while comparable information on hole transfer superexchange systems is quite scarce. Examples of multiatom ligands which do mediate metal−metal coupling via hole transfer superexchange include the malononitrile anion (MN$^-$),[5] the triazole anion,[6] the bibenzimidazolate dianion,[7] the tetrapyridylbiphenyl dianion,[8] and all of their respective derivatives. However, these ligands all act as both $\pi$-donors and $\pi$-acceptors, and the information they provide involves contributions from both pathways. One of the very few families of multiatom ligands which act purely as $\pi$-donors are the azodicarbonyl dianions.[9]

Optimal superexchange requires that metal and bridging-ligand orbitals have quite similar energies and, therefore, that the bonding be significantly covalent. Determining exactly how this can be purposefully achieved and recognized is a major goal of our research. Our approach has been to design a bridging ligand possessing a $\pi$-donor HOMO that spans the entire molecule. If the metal ions possess $\pi$d acceptor orbitals of the appropriate energy and orientation to interact with the bridging-ligand HOMO, then a continuous superexchange "$\pi$-

* Corresponding author.
[†] Carleton University.
[‡] University of Montreal.
[§] McMaster University.
[||] St. Petersburg University.
[⊗] Abstract published in *Advance ACS Abstracts,* June 15, 1997.

(1) (a) Manriquez, J. M.; Yee, G. T.; McLean, R. S.; Epstein, A. J.; Miller, J. S. *Science* **1991**, *252*, 1415. (b) Du, G.; Joo, J.; Epstein, A. J.; Miller, J. S. *J. Appl. Phys.* **1993**, *73*, 6566.
(2) (a) Aumuller, A.; Erk, P.; Klebe, G.; Hunig, S.; Von Schutz, J. U.; Werner, H.-P. *Angew. Chem., Int. Ed. Engl.* **1986**, *25*, 740. (b) Kato, R.; Kobayashi, H.; Kobayashi, A. *J. Am. Chem. Soc.* **1989**, *111*, 5224.
(3) (a) Kahn, O. *Molecular Magnetism;* VCH Publishers: New York, 1993. (b) Carlin, R. L. *Magnetochemistry*; Springer-Verlag: Berlin, Heidelberg, 1986.
(4) (a) Creutz, C. *Prog. Inorg. Chem*. **1983**, *30*, 1. (b) Crutchley, R. J. *Adv. Inorg. Chem*. **1994**, *41*, 273.
(5) Krentzien, H.; Taube, H. *J. Am. Chem. Soc*. **1976**, *98*, 6379.
(6) Hage, R.; Haasnoot, J. G.; Reedijk, J.; Wang, R.; Vos, J. G. *Inorg. Chem*. **1991**, *30*, 3263.
(7) (a) Haga, M.; Matsumura-Inoue, T.; Yamabe, S. *Inorg. Chem*. **1987**, *26*, 4148. (b) Haga, M.; Bond, A. M. *Inorg. Chem*. **1991**, *30*, 475. (c) Ohno, T.; Nozaki, K.; Haga, M. *Inorg. Chem*. **1992**, *31*, 4256. (d) Rillema, D. P.; Sahai, R.; Matthews, P.; Edwards, A. K.; Shaver, R. J. *Inorg. Chem*. **1990**, *29*, 167.
(8) Beley, M.; Collin, J.-P.; Louis, R.; Metz, B.; Sauvage, J.-P. *J. Am. Chem. Soc*. **1991**, *113*, 8521.
(9) (a) Kaim, W.; Kasack, V.; Binder, H.; Roth, E.; Jordanov, J. *Angew. Chem., Int. Ed. Engl*. **1988**, *27*, 1174. (b) Kaim, W. Kasack, V. *Inorg. Chem*. **1990**, *29*, 4696. (c) Kasack, V.; Kaim, W.; Binder, H.; Jordanov, J.; Roth, E. *Inorg. Chem*. **1995**, *34*, 1924.

S0020-1669(97)00026-8 CCC: $14.00 

way" for metal−metal coupling will result. The HOMO of the bridging ligand must be extremely polarizable and should resemble the atomic bridge $O^{2-}$ with its well-known capabilities of mediating metal−metal interactions in both molecular[10] and solid state materials.[11]

The bridging ligands that we have chosen are 1,4-dicyanamidobenzene dianion ($dicyd^{2-}$),

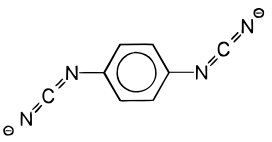

and its 2,5-dimethyl- ($Me_2dicyd^{2-}$), 2,5-dichloro- ($Cl_2dicyd^{2-}$), and 2,3,5,6-tetrachloro- ($Cl_4dicyd^{2-}$) substituted derivatives. We have explored the electronic properties of the cyanamide group and the ability of the $dicyd^{2-}$ bridging ligand to mediate metal−metal coupling in $[\{(NH_3)_5Ru\}_2(\mu\text{-dicyd})]^{3+/4+/5+}$ complexes.[12] These complexes are unique in the literature in that evidence for strong metal−metal coupling via the hole transfer mechanism was seen for Ru(III)−Ru(II),[12a,b] Ru(III)−Ru(III),[12b,c] and Ru(IV)−Ru(III)[12d] oxidation states. In addition, the dinuclear complexes $[\{(NH_3)_5Ru\}_2(\mu\text{-L})]^{3+/4+}$ where L is $dicyd^{2-}$ or $Me_2dicyd^{2-}$, showed remarkable solvent dependent metal−metal coupling.[12a,b] This latter property may have application to a molecular switching device, and we are currently devising synthetic techniques to construct conducting polymers which include Ru−dicyd−Ru linkages. The solvent dependence of metal−metal coupling in the mixed-valence complexes supports their classification as class II systems[13] albeit strongly coupled. The choice of spectator ligands for the five available coordination sites about ruthenium can "tune" the energy of ruthenium d$\pi$ orbitals and hence metal−metal superexchange via the $dicyd^{2-}$ bridging ligand to the point where class III properties are realized as has been shown for the mixed-valence complex $[\{Ru(trpy)(bpy)\}_2(\mu\text{-dicyd})]^{3+}$.[14]

In this study, the dinuclear Ru(III) complexes, *trans*-$[\{(NH_3)_4Ru(py)\}_2(\mu\text{-L})][PF_6]_4$, where py is pyridine and L = $dicyd^{2-}$ (**1**), $Me_2dicyd^{2-}$ (**2**), $Cl_2dicyd^{2-}$ (**3**), and $Cl_4dicyd^{2-}$ (**4**), have been prepared to examine the effect of the nature of the substituent on the $dicyd^{2-}$ bridging ligand on metal−metal coupling via Ru−dicyd−Ru linkages. The properties of these complexes will be compared with those of their pentaammine analogues and differences related to the perturbation of ruthenium d-orbital energies by pyridine and ammine ligands.

## Experimental Section

**Reagents.** All solvents and chemicals were reagent grade or better and used as received unless otherwise noted. Tetrabutylammonium bromide, TBAB, and tetrabutylammonium hexafluorophosphate, TBAH, were purchased from Aldrich. 1,4-Dicyanamidobenzene ($dicydH_2$), 1,4-dicyanamido-2,5-dimethylbenzene ($Me_2dicydH_2$), tetraphenylarsonium 1,4-dicyanamido-2,5-dichlorobenzene ($[AsPh_4]_2[Cl_2dicyd]$), and tetraphenylarsonium 1,4-dicyanamido-2,3,5,6-tetrachlorobenzene ($[AsPh_4]_2[Cl_4dicyd]$) were synthesized according to published procedures.[12c] *trans*-$[(NH_3)_4Ru(py)(H_2O)][PF_6]_2$, where py is pyridine, was prepared according to the method of Chang et al.[15] CM-Sephadex C25-120 cation exchange resin was purchased from Sigma.

**Preparation of [*trans*-$\{(NH_3)_4Ru(py)\}_2(\mu\text{-dicyd})][PF_6]_4\cdot H_2O$ (1).** A solution of *trans*-$[(NH_3)_4Ru(py)(H_2O)][PF_6]_4$ (280 mg) in 40 mL of acetone and another of $dicydH_2$ (40 mg) in 40 mL of acetone were prepared under an argon atmosphere. The solutions were then mixed and stirred with gentle heating (25−30 °C) overnight, during which time the solution's color changed from orange-red to a light green. The complex was then oxidized by exposure of the reaction solution to the atmosphere for 1 h and precipitated from the dark green solution as a bromide salt by the addition of 1.5 g of TBAB in 20 mL of acetone. The bromide salt was purified by ion exchange chromatography using Sephadex C-25. The loaded column was first eluted with 0.3 M NaCl, followed by 0.5 M and finally 1.0 M NaCl, and gave a yellow band, followed by a green-blue band (probably a mononuclear dicyd complex), and finally the grass-green band of the product. This was collected and the complex precipitated by the addition of excess ammonium hexafluorophosphate. The complex was recrystallized by ether diffusion into an acetonitrile solution of the complex, yielding green needles, 50 mg (16%). Anal. Calcd for $C_{18}H_{40}N_{14}OF_{24}P_4Ru_2$: C, 17.27; H, 3.19; N, 15.67. Found: C, 17.61; H, 2.99; N, 15.20. $\nu$(NCN) = 2086 $cm^{-1}$.

**Preparation of *trans*-$[\{(NH_3)_4Ru(py)\}_2(\mu\text{-Me}_2dicyd)][PF_6]_4$ (2).** This complex was prepared in the same manner as its $dicyd^{2-}$ analogue. The yield was 20%. Anal. Calcd for $C_{20}H_{42}N_{14}F_{24}P_4Ru_2$: C, 19.03; H, 3.33; N, 15.54. Found: C, 19.54; H, 3.38; N, 15.08. $\nu$(NCN) = 2084 $cm^{-1}$.

**Preparation of *trans*-$[\{(NH_3)_4Ru(py)\}_2(\mu\text{-Cl}_2dicyd)][PF_6]_4\cdot{}^1/_2(CH_3CH_2)_2O$ (3).** The poor solubility of $Cl_2dicydH_2$ in acetone required $[AsPh_4]_2[Cl_2dicyd]$ to be used instead. A solution of *trans*-$[(NH_3)_4Ru(py)(H_2O)][PF_6]_4$ (280 mg) in 50 mL of degassed acetone and another of $[AsPh_4]_2[Cl_2dicyd]$ (250 mg) in 450 mL of degassed acetone were prepared under an argon atmosphere. The $[AsPh_4]_2[Cl_2dicyd]$ solution had to be heated between 40 and 50 °C to keep the ligand in solution. The solutions were then mixed and stirred with gentle heating (25−30 °C) overnight. The precipitated $[AsPh_4][PF_6]$ was then filtered off and the filtrate reduced in volume to about 55 mL. The concentrated solution was exposed to air for 3 h, and then 2 g of TBAB was added, which precipitated the crude green bromide salt of the product. This was purified by ion exchange chromatography using Sephadex CM-25. The loaded column was first eluted with 1.0 M NaCl to separate three bands (grass-green, blue-green, and the deep green band of the product). The product band was eluted with 2.0 M NaCl and the eluent concentrated to approximately half its volume and placed in a refrigerator (4 °C) overnight, precipitating the chloride salt of the complex. This was filtered off, dissolved in a minimum volume of water, and metathesized to the $PF_6^-$ salt by the addition of excess $NH_4PF_6$. The complex was recrystallized by ether diffusion into an acetonitrile solution of the complex, yielding green microcrystals, 50 mg (15%). Anal. Calcd for $C_{20}H_{41}N_{14}O_{0.5}F_{24}P_4Cl_2Ru_2$: C, 17.95; H, 3.09; N, 14.65. Found: C, 17.68; H, 2.82; N, 14.81. $\nu$(NCN) = 2099 $cm^{-1}$.

**Preparation of *trans*-$[\{(NH_3)_4Ru(py)\}_2(\mu\text{-Cl}_4dicyd)][PF_6]_4$ (4).** This complex was prepared in the same manner as its $Cl_2dicyd^{2-}$ analogue. The yield was 5%. Anal. Calcd for $C_{18}H_{34}N_{14}F_{24}P_4Cl_4Ru_2$: C, 15.75; H, 2.48; N, 14.29. Found: C, 16.15; H, 2.59; N, 14.08. $\nu$(NCN) = 2110 $cm^{-1}$.

**Physical Measurements.** The equipment used to perform cyclic voltammetry, IR (KBr pellets), $^1$H-NMR, and UV−vis−near-IR spectroscopy has been described.[12b,16] Spectroelectrochemistry was performed with a Pyrex-quartz cell of published design,[17] on acetonitrile solutions containing approximately 0.03 mM dimer complex and 0.1 M TBAH electrolyte. Platinum-mesh working, platinum-wire counter, and silver-wire reference electrodes were used. The solutions were degassed and agitated by bubbling argon through a Teflon needle. The potential at the working electrode was controlled by using a BAS CV-

(10) Baumann, J. A.; Meyer, T. J. *Inorg. Chem.* **1980**, *19*, 345.
(11) Rao, C. N. R.; Raveau, B. *Transition Metal Oxides*; VCH Publishers: New York, 1995.
(12) (a) Naklicki, M. L.; Crutchley, R. J. *J. Am. Chem. Soc.* **1994**, *116*, 6045. (b) Naklicki, M. L.; Crutchley, R. J. *Inorg. Chim. Acta* **1994**, *225*, 123. (c) Aquino, M. A. S.; Lee, F. L.; Gabe, E. J.; Bensimon, C.; Greedan, J. E.; Crutchley, R. J. *J. Am. Chem. Soc.* **1992**, *114*, 5130. (d) Naklicki, M. L.; White, C. A.; Krondratiev, V.; Crutchley, R. J. *Inorg. Chim. Acta* **1996**, *242*, 63.
(13) Robin, M. B.; Day, P. *Adv. Inorg. Chem. Radiochem.* **1967**, *10*, 247.
(14) Rezvani, A. R.; Evans, C. E. B; Crutchley, R. J. *Inorg. Chem.* **1995**, *34*, 4600.
(15) Chang, J. P.; Fung, E. Y.; Curtis, J. C. *Inorg. Chem.* **1986**, *25*, 4233.
(16) Rezvani, A. R.; Crutchley, R. J. *Inorg. Chem.* **1994**, *33*, 170.
(17) Brewer, K. J.; Calvin, M.; Lummpkin, R. S.; Otvos, J. W.; Spreer, L. O. *Inorg. Chem.* **1989**, *28*, 4446.

27 apparatus. Aldrich anhydrous acetonitrile was used as received. TBAH was recrystallized twice from ethanol and vacuum dried at 110 °C overnight. Ferrocene ($E° = 665$ mV vs NHE)[18] was used as an internal reference in the cyclic voltammetry experiments. Elemental analysis was performed by Canadian Microanalytical Service Ltd. Temperature-dependent magnetic susceptibility measurements were performed on a Quantum Design SQUID magnetometer from 5 to 300 K in a 1.0 T field.

**Crystallography.** A plate crystal of *trans*-[{$(NH_3)_4Ru(py)$}$_2$($\mu$-dicyd)][$PF_6$]$_4$·$^1/_2H_2O$, having the dimensions 0.1 mm × 0.2 mm × 0.35 mm, was grown from a dilute acetonitrile solution by ether diffusion at approximately 4 °C over a period of 1 week. All of the measurements were made on a Rigaku diffractometer with Mo Kα radiation. Cell constants and an orientation matrix for data collection were obtained from least-squares refinement by using the setting angles of 25 reflections in the range $40° < 2\theta < 50°$ and corresponded to a monoclinic cell with dimensions $a = 7.826(3)$ Å, $b = 20.445(7)$ Å, and $c = 14.428(5)$ Å and $\beta = 95.76(3)°$. On the basis of systematic absences, the space group was determined to be $P2_1$ or $P2_1/m$. The structure was first solved in $P2_1$, and then the program Missym[19] was used in an attempt to discover any missing symmetry. To get to the space group $P2_1/m$ would require significant disorder, which, while possible for the $PF_6^-$ ion, would also require disorder in the ruthenium complex ion, and this seemed less likely. On this basis, the space group $P2_1$ was chosen over $P2_1/m$. The data were collected at −160 °C by using the $\omega-2\theta$ scan technique to a maximum $2\theta$ value of 49.9°.

A total of 4083 reflections were collected. The unique set contains only 3717 reflections. The standards were measured after every 150 reflections, and no crystal decay was noticed. The data were corrected for Lorentz and polarization effects.[20] An absorption correction was made using $\psi$ scan techniques. The minimum and maximum transmission factors are 0.4991 and 0.5827.

The structure was solved by direct methods. All of the atoms were refined anisotropically except the hydrogen atoms, which were calculated. The unobserved reflections were used during the refinement to increase the ratio of reflections per parameter. The final cycle of full-matrix least-squares refinement was based on 3292 observed reflections ($I > 2.5\sigma$(I)) and 563 variable parameters. Weights based on counting statistics were used. The maximum and minimum peaks on the final difference Fourier map corresponded to −1.320 and 1.490 Å$^{-3}$, respectively, corresponding to residuals at 1 Å of the two ruthenium atoms. All calculations were performed using the NRCVAX crystallographic software package.[21] The refinement of this crystal structure is slightly high with $R_f = 0.069$ and may result from crystal disorder due to the counterion $PF_6^-$.

The crystallography data and data collection parameters, atomic parameters, anisotropic thermal parameters, and final structure factors and a complete listing of bond lengths and angles are available as Supporting Information.

**Extended Hückel Calculations.** These were performed with the Quantum Chemistry Program Exchange program No. QCMP 011, Forticon 8 for personal computers.

**PKS Theory Calculations.** We used the dynamic mixed-valence model developed by Schatz et al. to estimate electronic and vibronic couplings from the intervalence band shapes.[22,23] The PKS model is defined in eqs 17−21 of ref 22. A time-dependent approach[24] was used to calculate a given spectrum. Equation 2 in ref 24 describes the PKS model and was used for our calculations, which include only transitions originating from the lowest energy vibronic level. This approximation is justified in view of the lack of a highly resolved intervalence band in our complexes and of the low thermal population of the next higher vibronic levels at room temperature. A vibrational energy of 450 cm$^{-1}$, in the range of Ru−N stretching modes,[22] was used for the calculations presented here, but a variation of up to 20% in the vibrational energies did not lead to drastic changes in band maxima and widths at half-height, which were determined numerically from our calculated spectra. A detailed discussion and comparison of different models involving only one coordinate, but including possible coordinate dependencies of the transition dipole moment for the intervalence band, has been published recently.[25]

**Table 1.** Crystal Data for *trans*-[{$(NH_3)_4Ru(py)$}$_2$($\mu$-dicyd)][$PF_6$]$_4$·$^1/_2H_2O$

| | |
|---|---|
| empirical formula | $C_{18}H_{38}N_{14}F_{24}P_4Ru_2 + {}^1/_2H_2O$ |
| fw | 1240.58 |
| cryst syst | monoclinic |
| space group | $P2_1$ |
| cryst dimens (mm) | 0.10 × 0.20 × 0.35 |
| $a$, Å | 7.826(3) |
| $b$, Å | 20.445(7) |
| $c$, Å | 14.428(5) |
| $\beta$, deg | 95.76(3) |
| $V$, Å$^3$ | 2296.7(14) |
| $Z$ | 2 |
| $\rho_{cald}$, g/cm$^3$ | 1.794 |
| $T$, °C | −160 |
| radiation ($\lambda$, Å) | Mo Kα (0.709 30) |
| $\mu$, mm$^{-1}$ | 0.91 |
| measd rflcns | 4038 |
| unique rflcns | 3717 |
| rflns ($I > 2.5\sigma(I)$) | 3292 |
| $R_f$[a] (signif refl) | 0.069 |
| $R_w$[b] (signif refl) | 0.088 |
| goodness-of-fit ratio | 3.40 |

[a] $R_f = \Sigma||F_o| - |F_c||/\Sigma|F_o|$. [b] $R_w = (\Sigma w(|F_o| - |F_c|)^2/\Sigma w|F_o|^2)^{1/2}$.

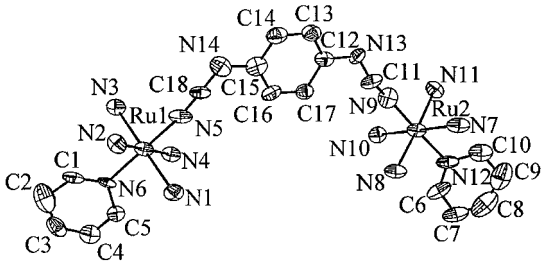


**Figure 1.** ORTEP drawing for the complex *trans*-[$(NH_3)_4Ru(py)$}$_2$-($\mu$-dicyd)][$PF_6$]$_4$·$^1/_2H_2O$. The $PF_6^-$ ions and $H_2O$ have been omitted for clarity.

## Results

Crystal structure data for *trans*-[{$(NH_3)_4Ru(py)$}$_2$($\mu$-dicyd)]$^{4+}$ are given in Table 1. Figure 1 shows the coordination geometry of the ligands about the Ru(III) ions and the atom-numbering scheme used to describe the corresponding bond lengths and bond angles in Table 2.

As shown by Figure 1, the two cyanamide groups of the bridging ligand are in a syn configuration, approximately coplanar with the phenyl ring plane. This is in contrast to the crystal structure of [{$(NH_3)_5Ru$}$_2$($\mu$-dicyd)]$^{4+}$ [12c] and those of the free 1,4-dicyanamidobenzene dianion ligands,[26] where the cyanamide groups adopted an anti configuration, coplanar with the phenyl ring plane. In the crystal structure of *trans*-[{$(NH_3)_4$-$Ru(py)$}$_2$($\mu$-dicyd)]$^{4+}$, one of the cyanamide planes formed by N9−C11−N13 is tilted by only 9° with respect to the plane of the phenyl ring. The other cyanamide plane formed by N5−C18−N14 is tilted out of the phenyl ring plane by 29°. The data in Table 2 show that the Ru(III) ions are approximately equivalent, with Ru(III)−NCN bond lengths of Ru1−N5 =

(18) Gennett, T.; Milner, D. F.; Weaver, M. J. *J. Phys. Chem.* **1985**, *89*, 2787.
(19) Lepage, Y. *J. Appl. Crystallogr.* **1988**, *21*, 983.
(20) Grant, D. F.; Gabe, E. J. *J. Appl. Crystallogr.* **1978**, *11*, 114.
(21) Gabe, E. J.; Lee, F. L.; Lepage, Y. *J. Appl. Crystallogr.* **1989**, *22*, 384.
(22) Piepho, S.; Krausz, E. R.; Schatz, P. N. *J. Am. Chem. Soc.* **1978**, *100*, 2996.
(23) Wong, K. Y.; Schatz, P. N. *Prog. Inorg. Chem.* **1981**, *28*, 369.
(24) Talaga, D. S.; Reber, C.; Zink, J, I. *J. Phys. Chem.* **1994**, *98*, 11233.
(25) Talaga, D. S.; Zink, J. I. *J. Chem. Phys.*, in press.
(26) Aquino, M. A. S.; Crutchley, R. J.; Lee, F. L.; Gabe, E. J.; Bensimon, C. *Acta Crystallogr.* **1993**, *C49*, 1543.

**Table 2.** Selected Crystal Structure Data[a] for *trans*-[{$(NH_3)_4Ru(py)$}$_2$($\mu$-dicyd)][$PF_6$]$_4$·$^1/_2H_2O$

| | | | |
|---|---|---|---|
| | Bond Lengths, Å | | |
| Ru1−N1 | 2.154(14) | Ru1−N2 | 2.135(16) |
| Ru1−N3 | 2.144(15) | Ru1−N4 | 2.152(15) |
| Ru1−N5 | 1.943(16) | Ru1−N6 | 2.060(14) |
| Ru2−N7 | 2.140(16) | Ru2−N8 | 2.128(14) |
| Ru2−N9 | 1.987(17) | Ru2−N10 | 2.126(16) |
| Ru2−N11 | 2.112(15) | Ru2−N12 | 2.055(16) |
| N5−C18 | 1.215(3) | N9−C11 | 1.10(3) |
| N14−C18 | 1.28(3) | N13−C11 | 1.307(24) |
| N14−C15 | 1.41(3) | N13−C12 | 1.34(3) |
| | Bond Angles, deg | | |
| N1−Ru1−N2 | 87.6(6) | N1−Ru1−N3 | 179.2(6) |
| N6−Ru1−N5 | 179.5(6) | N6−Ru1−N4 | 90.4(6) |
| Ru1−N5−C18 | 171.0(16) | N5−C18−N14 | 178.4(19) |
| N7−Ru2−N8 | 89.1(6) | N7−Ru2−N10 | 179.7(6) |
| N9−Ru2−N12 | 176.1(7) | N12−Ru2−N8 | 90.3(6) |
| Ru2−N9−C11 | 174.3(15) | N9−C11−N13 | 167.1(23) |

[a] The atom numbers are shown in Figure 1, and the numbers in parentheses are estimated standard deviations.

**Table 3.** Electronic Absorption Data[a] for the *trans*-[{$(NH_3)_4Ru(py)$}$_2$($\mu$-L)]$^{4+}$ Complexes in Acetonitrile

| L | $\pi^* \leftarrow \pi$ | LMCT transitions |
|---|---|---|
| $Me_2dicyd^{2-}$ | 244 (4.16), 290 (4.01) | 378 (4.18), 1126 (4.88) [1860] |
| $dicyd^{2-}$ | 250 (4.27), 274 (4.25) | 379 (4.08), 1163 (4.88) [1730] |
| $Cl_2dicyd^{2-}$ | 248 (4.36), 280 (4.34) | 393 (4.02), 1176 (4.73) [2020] |
| $Cl_4dicyd^{2-}$ | 225 (4.09), 297 (4.34) | 407 (3.91), 1069 (4.42) [4450] |

[a] Wavelength in nm with log $\epsilon$ ($\epsilon$ in $M^{-1}$ $cm^{-1}$) in parentheses and band width at half peak height ($\Delta\nu_{1/2}$ in $cm^{-1}$) in square brackets.

1.943(16) Å and Ru2−N9 = 1.987(17) Å. However, the bond lengths and angles of the cyanamide groups in Table 2 suggest a dominant contribution from resonance form A to the cyanamide group coordinated to Ru1 and an increased contribution from resonance form B to the cyanamide group coordinated to Ru2.

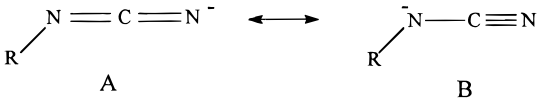


The inequivalence of the Ru(III) coordination spheres and the distortion of the $dicyd^{2-}$ ligand from ideal planar geometry are probably due to crystal-packing forces and the hydrogen-bonding interactions of the water of crystallization which is in hydrogen-bonding contact to the protons of N8, N10, and C17 (2.05, 2.46, and 2.64 Å, respectively). The Ru1−Ru2 through space distance, 10.9 Å, is considerably shorter than the 13.1 Å found for [{$(NH_3)_5Ru$}$_2$($\mu$-dicyd)]$^{4+}$.[12c]

UV−vis−near-IR electronic absorption data for the complexes are compiled in Table 3 and a spectrum of the Ru(III)−Ru(III) complex *trans*-[{$(NH_3)_4Ru(py)$}$_2$($\mu$-$Cl_2$dicyd)]$^{4+}$ is shown in Figure 2. Spectroscopic analyses[27] of the Ru(III)−NCN chromophore have shown that two ligand-to-metal charge transfer (LMCT) transitions can be expected. These LMCT transitions arise from two nondegenerate pairs of nonbonding electrons that are delocalized in the cyanamide moiety. Spectroelectrochemistry studies were also performed on complexes **1**−**4** to obtain the electronic spectra of the corresponding Ru(III)−Ru(II) complexes. The reduction of complex **3** to form *trans*-[{$(NH_3)_4Ru(py)$}$_2$($\mu$-$Cl_2$dicyd)]$^{3+}$ is shown in Figure 2. The reduction of these complexes was reversible, as evidenced

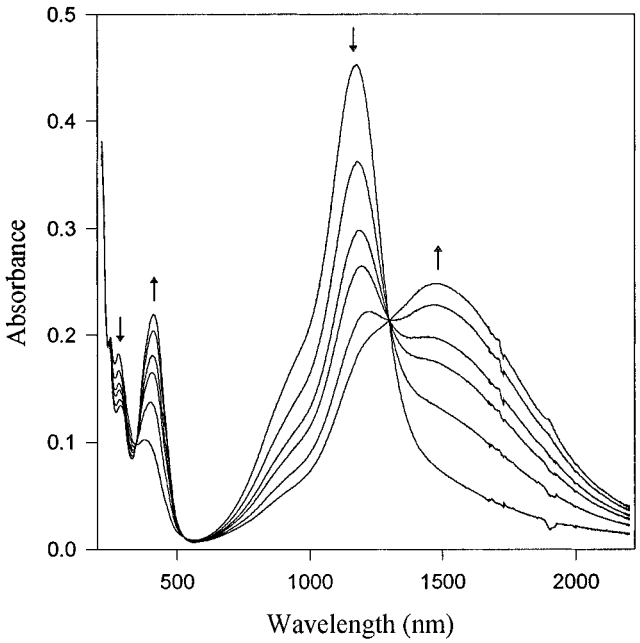


**Figure 2.** Spectroelectrochemical reduction of *trans*-[{$(NH_3)_4Ru(py)$}$_2$-($\mu$-$Cl_2$dicyd)]$^{4+}$ (**3**) in acetonitrile.

**Table 4.** Intervalence Band Data[a] of the *trans*-[{$(NH_3)_4Ru(py)$}$_2$($\mu$-L)]$^{3+}$ Complexes in Acetonitrile

| L | $R^2$ [b] | $\nu_{max}$ ($cm^{-1}$) | $\epsilon_{max}$ ($M^{-1}$ $cm^{-1}$) | $\Delta\nu_{1/2}$ ($cm^{-1}$) |
|---|---|---|---|---|
| $Me_2dicyd^{2-}$ | 0.976 | 7410 | 22300 | 1640 |
| $dicyd^{2-}$ | 0.952 | 7130 | 25500 | 1900 |
| $Cl_2dicyd^{2-}$ | 0.998 | 6630 | 21800 | 2560 |
| $Cl_4dicyd^{2-}$ | 0.994 | 6520 | 17900 | 3200 |

[a] Deconvoluted from the LMCT band envelope using Peakfit version 3 software assuming that the IT transition results in a single gaussian band and no change in either energy or band shape of the LMCT transtion. See ref 12b for details. [b] Square of the correlation coefficient for the least squares fit of the absorption band envelope.

by the maintenance of isosbestic points and the regeneration of the Ru(III)−Ru(III) spectra upon oxidation. Further reduction to the Ru(II)−Ru(II) complexes proved irreversible, with only partial recovery of the absorption spectra of the Ru(III)−Ru(III) complexes. Nevertheless, it was apparent that the Ru(II)−Ru(II) complexes do not significantly absorb at wavelengths greater than 600 nm. In Figure 2, the growth of the low-energy band with the formation of the mixed-valence complex is therefore assigned to an intervalence transition (IT). This transition was deconvoluted from the LMCT band envelope by using methods that have already been discussed in detail.[12b] The main assumptions are that the IT can be represented by a single Gaussian band and that the LMCT band does not change its energy upon formation of the Ru(III)−Ru(II) complex. The IT band data for the mixed-valence complexes are summarized in Table 4.

Cyclic voltammetry data for the complexes in acetonitrile solution have been placed in Table 5, and a representative cyclic voltammogram is shown in Figure 3. The four waves (Figure 3) have been assigned on the basis of previous studies of mononuclear phenyl cyanamide ruthenium complexes[28] and cyclic voltammetry studies of the free $dicyd^{2-}$ ligands.[29,30] The two waves at negative potential are formally assigned to the two Ru(III/II) reduction couples, and the two ligand reduction

(27) (a) Crutchley, R. J.; Naklicki, M. L. *Inorg. Chem.* **1989**, *28*, 1955. (b) Evans, C. E. B.; Ducharme, D.; Naklicki, M. L.; Crutchley, R. J. *Inorg. Chem.* **1995**, *34*, 1350.

(28) Crutchley, R. J.; McCaw, K.; Lee, F. L.; Gabe, E. J. *Inorg. Chem.* **1990**, *29*, 2576.

(29) Aumuller, A.; Hunig, S. *Liebigs Ann. Chem.* **1986**, 142.

(30) Aquino, M. A. S. Ph.D. Thesis, Carleton University, 1991. Naklicki, M. L. Ph.D. Thesis, Carleton University, 1995.

**Table 5.** Cyclic Voltammetry Data[a] of the *trans*-[{$(NH_3)_4Ru(py)$}$_2$($\mu$-L)]$^{4+}$ Complexes in Acetonitrile

| L | Ru(III/II) | Ru(III/II) | $K_c$[b] | L(−/2−) | L(0/−) |
|---|---|---|---|---|---|
| $Me_2dicyd^{2-}$ | 0.315 | −0.085 | $5.8 \times 10^6$ | 0.935 | 1.265 |
| $dicyd^{2-}$ | 0.350 | −0.015 | $1.5 \times 10^6$ | 0.965 | 1.340 |
| $Cl_2dicyd^{2-}$ | 0.410 | 0.165 | $1.4 \times 10^4$ | 1.045 | 1.455[c] |
| $Cl_4dicyd^{2-}$ | 0.435 | 0.255 | $1.1 \times 10^3$ | 1.170 | 1.595[c] |

[a] Volts vs NHE at a scan rate of 100 mV $s^{-1}$; in 0.1 M TBAH acetonitrile. [b] $\log K_c = \Delta E/0.05915$, where $\Delta E$ is the difference between Ru(III/II) couples. [c] Irreversible, anodic wave maximum reported.

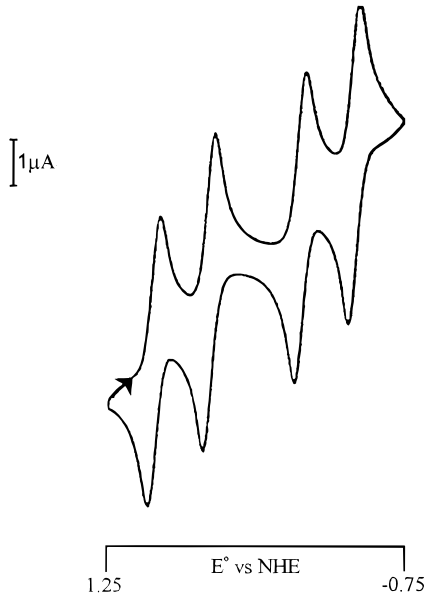


**Figure 3.** Cyclic voltammogram of *trans*-[{$(NH_3)_4Ru(py)$}$_2$($\mu$-dicyd)]$^{4+}$ in acetonitrile, 0.1 M TBAH, at 100 mV/s.

couples (L(0/−) and L(−/2−)) are assigned to the two waves that appear at more positive potentials. The assignment of the L(−/2−) couple may actually correspond to a Ru(IV/III) couple on the basis of spectroelectrochemical oxidation studies of the [{$(NH_3)_5Ru$}$_2$($\mu$-$Me_2$dicyd)]$^{4+}$ complex.[12d] A specific assignment is difficult because of the increased covalent character of the Ru−NCN bond in [{$(NH_3)_5Ru$}$_2$($\mu$-$Me_2$dicyd)]$^{5+}$. The Ru(III/II) waves for all of the dinuclear complexes appear reversible with an average separation between cathodic and anodic waves of 60 mV that is independent of scan rate between 50 and 500 mV/s and anodic to cathodic current ratios that are close to unity. This is also true for the first ligand redox couple (L(−/2−)) in all of the complexes and the second couple (L(0/−)) of complexes **1** and **2**. Only an anodic peak is observed for the L(0/−) couple of complexes **3** and **4**.

From the difference between the two Ru(III/II) reduction couples can be calculated the comproportionation constant $K_c$ for the reaction,

$$\text{Ru(III)}-\text{Ru(III)} + \text{Ru(II)}-\text{Ru(II)} \overset{K_c}{\rightleftharpoons} 2\text{Ru(III)}-\text{Ru(II)} \quad (1)$$

These values have been placed in Table 5.

Magnetic susceptibility measurements of the Ru(III)−Ru(III) complexes were made over the temperature range 5−300 K. All of the complexes were diamagnetic at room temperature and showed only a weak paramagnetic tail at low temperatures due to a paramagnetic impurity. Unfortunately, the complexes are thermally unstable at temperatures greater than 400 K, and so an exact determination of the exchange constant is not possible. An estimate of the intramolecular antiferromagnetic exchange constant for these complexes is $-J \geq 500$ $cm^{-1}$, where $H = -2JS_a \cdot S_b$.

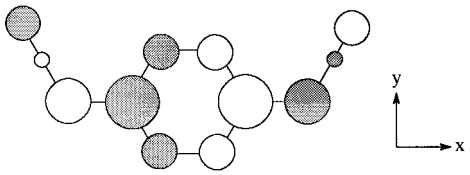


**Figure 4.** The $\pi_{nb}$ HOMO of $dicyd^{2-}$ in the syn conformation as determined by extended Hückel calculations. Only the $p_z$ orbital contributions are shown, with other minor orbital contributions omitted for clarity and phase differences represented by shading.

## Discussion

A comprehensive description of superexchange metal−metal coupling in dinuclear transition metal complexes should consider the entire set of bridging ligand molecular orbitals to take into account both hole transfer and electron transfer superexchange mechanisms. Nevertheless, it is possible to simplify matters by selecting a bridging ligand for which either hole transfer or electron transfer superexchange is optimized. If there is a strong bonding interaction between metal orbitals and a commonly shared *unoccupied* bridging ligand orbital, low-energy metal-to-ligand charge transfer will be observed in the compound's absorption spectrum and the dominant superexchange mechanism will be electron transfer. On the other hand, if there is a strong bonding interaction between metal orbitals and a commonly shared *occupied* bridging ligand orbital, low-energy ligand-to-metal charge transfer will be observed and the dominant superexchange mechanism will be hole transfer.

For the complexes of this study, metal−metal coupling is suggested to occur via hole transfer superexchange involving the $\pi_{nb}$ HOMO of the $dicyd^{2-}$ bridging ligand. Extended Huckel calculations of the $dicyd^{2-}$ ligand, assuming ideal planar geometry with cyanamide groups in either anti[30] or syn conformations, revealed $\pi$ symmetry HOMOs that were essentially identical in appearance and energy at this level of theory. Figure 4 shows the result of these calculations for the $dicyd^{2-}$ ligand in the syn conformation. It is important to note that the HOMO spans the entire bridging ligand and is therefore able to interact simultaneously with the d$\pi$ orbitals of both ruthenium ions and that it is largely constituted from $p_z$ orbital contributions. These bridging-ligand properties optimize superexchange, and this is dramatically illustrated by the room temperature diamagnetism that is seen for all of the Ru(III)−Ru(III) complexes with $-J \geq 500$ $cm^{-1}$, a result that has been observed previously for only the most strongly coupled pentaammineruthenium dimer, [{$(NH_3)_5Ru$}$_2$($\mu$-$Me_2$dicyd)]$^{4+}$.[12c] In addition, to underscore the importance of a planar geometry, a crystal structure of the 1,4-dicyanamido-2,3,5,6-tetramethylbenzene dianion ligand $Me_4dicyd^{2-}$ showed the cyanamide groups to be still in an anti conformation but forced out of the phenyl ring plane.[31] Extended Hückel calculations showed the HOMO to be largely localized to the phenyl ring, and as a consequence, intramolecular antiferromagnetic exchange in [{$(NH_3)_5Ru$}$_2$($\mu$-$Me_4$dicyd)]$^{4+}$ was significantly attenuated[31] with $-J = 53$ $cm^{-1}$ when compared to the analogous $dicyd^{2-}$ complexes.[12c]

Strong metal−metal coupling in the mixed-valence complexes of **1**−**4** is demonstrated by the magnitude of the comproportionation constants found in Table 5. For the pentaammine−ruthenium complexes [{$(NH_3)_5Ru$}$_2$($\mu$-dicyd)]$^{3+}$ [12b] and [{$(NH_3)_5Ru$}$_2$($\mu$-$Me_2$dicyd)]$^{3+}$,[12a] the comproportionation constants in acetonitrile were determined to be $6.8 \times 10^4$ and $5.6 \times 10^5$, respectively. These values are significantly smaller than those

(31) Aquino, M. A. S.; Lee, F. L.; Gabe, E. J.; Greedan, J. E.; Crutchley, R. J. *Inorg. Chem.* **1991**, *30*, 3234.

**Table 6.** Metal−Ligand and Metal−Metal Coupling Elements[a] for the Ru(III)−Ru(II) Complexes *trans*-[{$(NH_3)_4$Ru(py)}$_2$($\mu$-L)]$^{3+}$

| | CNS model | | | hush model | | PKS model | | expt |
|---|---|---|---|---|---|---|---|---|
| L | $H_{LM}$[b] | $\Delta E_{LM}$[c] | $H_{MM'}$[d] | $\Delta\nu_{1/2}$[e] | $H_{ad}$[f] | $\lambda$[g] | $-\epsilon$[g] | $\Delta G_r$[h] |
| $Me_2$dicyd$^{2-}$ | 3600 | 3520 | 5100 | 4140 | 980 | 1.5 | 7.1 | 2750 |
| dicyd$^{2-}$ | 3400 | 2510 | 4600 | 4060 | 1110 | 1.9 | 6.7 | 2460 |
| $Cl_2$dicyd$^{2-}$ | 3000 | 3060 | 2900 | 3910 | 1150 | 2.4 | 6.2 | 1500 |
| $Cl_4$dicyd$^{2-}$ | 3300 | 4360 | 2500 | 3880 | 1150 | 3.0 | 5.5 | 970 |

[a] All data are in cm$^{-1}$ except $\lambda$ and $\epsilon$, which are dimensionless. [b] Calculated according eq 4, assuming $r = 6.5$ Å and using the data in Table 3. [c] Calculated according to eq 8, using the data in Tables 3 and 4. [d] Calculated according to eq 6. [e] Calculated according to eq 5, using the data in Table 4. [f] Calculated according to eq 4, assuming $r = 10.9$ Å and using the data in Table 4. [g] Obtained from numerical calculations as shown in Figure 6 and disscussed in the Experimental Section. [h] $\Delta G_r = \Delta G_c - 480$ cm$^{-1}$, using the $K_c$ values in Table 5. See text for details.

for complexes **1** and **2** in Table 6 and must be associated with the replacement of an ammine ligand by pyridine. Because the ammine ligand is a stronger donor of electron density than pyridine, the Ru(III) d$\pi$ orbitals are destabilized to a greater extent, and this increases the energy gap between Ru(III) d$\pi$ and the HOMO of the dicyd$^{2-}$ ligand. This increase in the energy gap reduces superexchange metal−metal coupling for the pentaammineruthenium dimers.

The mixed-valence complexes of **1**−**4** are classified as class II systems because of a strong solvent dependence similar to that seen for their pentaammine analogues.[12a,b] For example, the comproportionation constants of **1**, **2**, **3** and **4** in aqueous solution are reduced to 47, 39, 29, and 10, respectively, compared to those obtained in acetonitrile (Table 5). This dramatic loss of coupling is suggested to arise from the high polarizability of these mixed-valence complexes and a preferred donor−acceptor interaction between the solvent and ammine ligands bound to Ru(III).[32] It is interesting to speculate about the magnitude of comproportionation constant that would be consistent with full delocalization and class III properties. The Creutz−Taube ion, [{$(NH_3)_5$Ru}$_2$($\mu$-pyrazine)]$^{5+}$, has been studied extensively, with the majority of evidence supporting a class III assignment for this ion. Its comproportionation constant has been found to be $1.9 \times 10^7$ in acetonitrile.[33] This value is close to those found in Table 5 for complexes **1** and **2** and suggests a considerable degree of delocalization in these complexes.

The comproportionation constant $\Delta G_c$ is only a qualitative measure of metal−metal coupling, and this is illustrated by the expression

$$\Delta G_c = \Delta G_s + \Delta G_e + \Delta G_i + \Delta G_r \qquad (2)$$

where $\Delta G_s$ is an entropy factor which reflects the statistical distribution of eq 1, $\Delta G_e$ accounts for the electrostatic repulsion of the two like-charged metal centers, $\Delta G_i$ is an inductive factor dealing with the competitive coordination by metal ions for the bridging ligand, and $\Delta G_r$ is the free energy of resonance exchange, the only component of $\Delta G_c$ which represents "actual" metal−metal coupling. All four terms can contribute significantly to $\Delta G_c$ for the weak coupling case;[34] however, in the case of the strongly coupled systems of this study, the resonance exchange term dominates $\Delta G_c$. An estimate of the nonresonance exchange contribution to the free energy of comproportionation,

$$\Delta G_{nr} = \Delta G_s + \Delta G_e + \Delta G_i \qquad (3)$$

for the complexes of this study can be obtained from the solvent dependent metal−metal coupling of *trans*-[{$(NH_3)_4$Ru(py)}$_2$-($\mu$-$Cl_4$dicyd)]$^{3+}$ in aqueous solution which was found to have $K_c = 10$ or $\Delta G_c = 480$ cm$^{-1}$. If it is assumed that $\Delta G_r$ is very small for *trans*-[{$(NH_3)_4$Ru(py)}$_2$($\mu$-$Cl_4$dicyd)]$^{3+}$ in aqueous solution,[35] then the magnitude of $\Delta G_c$ will be largely determined by the $\Delta G_{nr}$ contributions. By subtracting $\Delta G_{nr} = 480$ cm$^{-1}$ from $\Delta G_c$, an experimental estimate of $\Delta G_r$ for each of the *trans*-[{$(NH_3)_4$Ru(py)}$_2$($\mu$-L)]$^{3+}$ complexes can be obtained. These have be placed in Table 6 for comparsion with metal−metal coupling energies that have been derived from theory.

It is important to recognize that the trend in $\Delta G_r$ for complexes **1**−**4** (Table 6) is consistent with the expected dependence of hole transfer superexchange on the energy gap between the $\pi_{nb}$ HOMO of the dicyd$^{2-}$ bridging ligand and ruthenium d$\pi$ orbitals. Increasing the number of electron-donating substituents on dicyd$^{2-}$ destabilizes the $\pi_{nb}$ HOMO, decreasing the energy gap and creating favorable conditions for superexchange. We now take this opportunity to examine the complexes of this study by theory and to compare the results against those experimentally determined.

The first model that we will consider is the perturbation theory derived Hush model for weakly coupled mixed-valence complexes[36] in which the IT band properties can be related to the magnitude of metal−metal coupling $H_{ad}$ by the expression

$$H_{ad} = \frac{2.06 \times 10^{-2}(\nu_{max}\epsilon_{max}\Delta\nu_{1/2})^{1/2}}{r} \qquad (4)$$

where $\nu_{max}$ is the IT band maximum in cm$^{-1}$, $\epsilon_{max}$ is the IT band maximum extinction coefficient in M$^{-1}$ cm$^{-1}$, $\Delta\nu_{1/2}$ is the IT band width at one-half $\epsilon_{max}$ in cm$^{-1}$, and $r$ is the transition moment length, which is usually taken to be the metal−metal separation in Å. In addition, the Hush model can be used to predict intervalence band width according to

$$\Delta\nu_{1/2} = (2310\nu_{max})^{1/2} \qquad (5)$$

By using the data in Table 4 and assuming that $r = 10.9$ Å (the crystal structure metal−metal separation), values of $H_{ad}$ and $\Delta\nu_{1/2}$ for each of the complexes were calculated and these have been placed in Table 6. Good agreement between $H_{ad}$ and $\Delta G_r$ in Table 6 and the $\Delta\nu_{1/2}$ values in Tables 4 and 6 is seen only for complex **4** and suggests that this complex with $\Delta G_r = 970$ cm$^{-1}$ can still be considered weakly coupled. However, the trends in $H_{ad}$ and calculated $\Delta\nu_{1/2}$ are opposite that seen for $\Delta G_r$ and the experimental $\Delta\nu_{1/2}$ in Table 4 and suggest a departure from weakly coupled to more strongly coupled systems for which the Hush model is inappropriate. The decreasing value of $H_{ad}$ with increasing $\Delta G_r$ is the result of decreasing IT oscillator strength. That this should occur with increasing metal−metal coupling may be due to the partial delocalization of the odd electron, which reduces the transition dipole moment length.

Creutz, Newton, and Sutin (CNS) have recently devised a model for metal−metal coupling $H_{MM'}$ in mixed-valence

(32) (a) Blackbourn, R. L.; Hupp, J. T. *Chem. Phys. Lett*. **1988**, *150*, 399. (b) Blackbourn, R. L.; Hupp, J. T. *J. Phys. Chem*. **1990**, *94*, 1790.
(33) Creutz, C.; Chou, M. H. *Inorg. Chem*. **1987**, *26*, 2995.
(34) Sutton, J. E.; Taube, H. *Inorg. Chem*. **1981**, *20*, 3125.
(35) The value of $\Delta G_r$ in aqueous solution may be canceled out by the increase in $\Delta G_e$ that is expected in acetonitrile solution. See: Ferrere, S.; Elliott, C. M. *Inorg. Chem*. **1995**, *34*, 5818. In addition, variations in $\Delta G_i$ for the complexes of this study are apparently not important, based on the linear relationship that is seen in Figure 5.
(36) (a) Hush, N. S. *Prog. Inorg. Chem*. **1967**, *8*, 391. (b) Hush, N. S. *Trans. Faraday Soc*. **1961**, *57*, 557. (c) Hush, N. S. *Electrochim. Acta* **1968**, *13*, 1005.

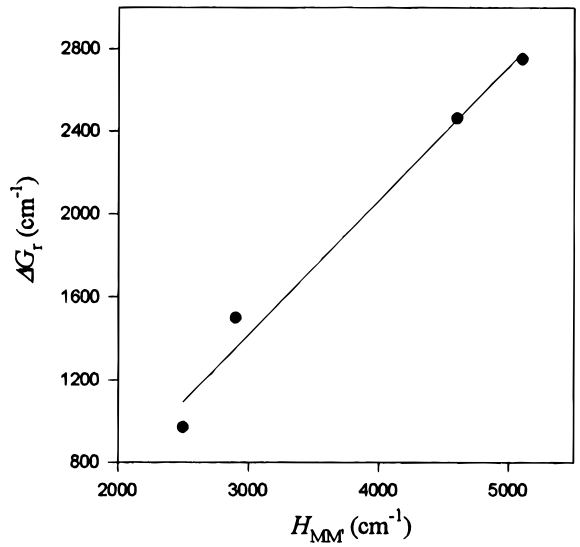


**Figure 5.** Plot of $\Delta G_r$ vs $H_{MM'}$ for *trans*-[{$(NH_3)_4Ru(py)$}$_2$($\mu$-L]$^{3+}$, L = dicyd$^{2-}$, Me$_2$dicyd$^{2-}$, Cl$_2$dicyd$^{2-}$, and Cl$_4$dicyd$^{2-}$. Values of $\Delta G_r$ and $H_{MM'}$ are found in Table 6. The line has slope = 0.65, intercept = $-520$ cm$^{-1}$, and $R^2 = 0.98$.

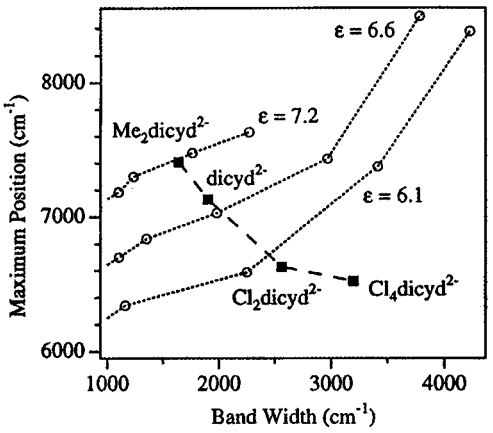


**Figure 6.** Comparison of calculated and experimental intervalence band maxima and band widths for *trans*-[{$(NH_3)_4Ru(py)$}$_2$($\mu$-L]$^{3+}$, L = dicyd$^{2-}$, Me$_2$dicyd$^{2-}$, Cl$_2$dicyd$^{2-}$, and Cl$_4$dicyd$^{2-}$. Solid squares denote experimental data with L as given next to the data point. Open circles denote calculated band widths and maxima. Dotted lines connect calculated results obtained with constant electronic coupling $\epsilon$ and variable vibronic coupling $\lambda$. All numerical values are given in Table 6.

complexes based on metal−bridging ligand coupling elements.[37] The general expression

$$H_{MM'} = \frac{H_{ML}H_{M'L}}{2\Delta E_{ML}} + \frac{H_{LM}H_{LM'}}{\Delta E_{LM}} \quad (6)$$

considers both electron and hole transfer superexchange pathways.[38] Evaluating the metal−ligand electronic coupling elements $H_{ML}$ or $H_{LM}$ from MLCT or LMCT band properties, respectively, is accomplished using eq 4. $\Delta E_{ML}$ and $\Delta E_{LM}$ represent the energetic difference between the metal orbitals and respectively the ligand $\pi^*$ LUMO and $\pi$ HOMO orbitals. Following the same reasoning as CNS,[37] the first term in eq 6 is taken to be 0 for $\pi$ donor ligand−metal interactions (which only exhibit LMCT transitions in the visible region). Equation 6 is further simplified by assuming that, for symmetric systems, $H_{LM} \approx H_{LM'}$, giving

$$H_{MM'} = H_{LM}{}^2/\Delta E_{LM} \quad (7)$$

The values of $\Delta E_{LM}$ in cm $^{-1}$ were calculated according to

$$1/\Delta E_{LM} = 0.5[1/E_{LMCT} + 1/(E_{LMCT} - E_{IT})] \quad (8)$$

where $E_{LMCT}$ is the energy of the lowest energy LMCT band (in Table 3) and $E_{IT}$ is the energy of the IT band ($\nu_{max}$ in Table 4). $H_{LM}$ was evaluted by using the data for the lowest energy LMCT band from Table 3 and eq 4, assuming $r = 6.5$ Å, the distance from a ruthenium ion to the center of the dicyd$^{2-}$ ligand. The results of these calculations have been placed in Table 6, and while it is clear that the values of $H_{MM'}$ overestimate $\Delta G_r$ by approximately a factor of 1.5, there is a rather good correlation as shown by Figure 5. The error in $H_{MM'}$ is likely due in part to the approximation $H_{LM'} \approx H_{LM}$. For optical electron transfer, the $H_{LM'}$ values derived from eq 4 are the values of the Ru(III)−L coupling elements for Ru(III) at the equilibrium configuration of Ru(II). These $H_{LM'}$ values will be smaller than $H_{LM}$ to the extent that Ru(II)−NCN bond lengths are expected to be longer than Ru(III)−NCN bond lengths. This correction could substantially reduce $H_{MM'}$.

The final approach to IT band properties that will be examined is the vibronic model developed by Schatz et al. (PKS) involving a single vibrational mode.[22,23] The details of our calculations with this model are given in the Experimental Section. The electronic coupling $\epsilon$ and the vibronic displacement $\lambda$ of the potential minima along the coordinate axis were adjusted to reproduce the band maxima and widths of the IT bands. Calculations with the PKS model using a constant $\epsilon$ and a variable $\lambda$ are compared to the experimental data in Figure 6, and it is clear that both $\epsilon$ and $\lambda$ must be varied to fit the experimental data. Our values of $\lambda$ and $\epsilon$ are in the same range as the values of $\lambda = 2.7$ and $\epsilon = 6$ obtained from a detailed band-shape analysis of the Creutz−Taube ion in ref 22. For complexes **1**−**3**, the variation of the electronic coupling is more important than the change in $\lambda$ and the spectrum of complex **4** can be rationalized with electronic coupling similar to that of complex **3** but a significantly higher vibronic coupling $\lambda$. The PKS model therefore allows a qualitative characterization of intervalence systems based on the parameters of their IT bands and points out the importance of vibronic effects.[39] It is reassuring to note that the same qualitative variation with L is observed for both $\epsilon$ and $\Delta G_r$, as summarized in Table 6.

## Conclusion

Whether the cyanamide groups are in a syn or anti conformation, the planar dicyd$^{2-}$ bridging ligand is an effective mediator of antiferromagnetic Ru(III)−Ru(III) exchange, as shown by solid state magnetic susceptibility studies of the [{$(NH_3)_5Ru$}$_2$-($\mu$-dicyd)]$^{4+}$ complexes[12c] and the *trans*-[{$(NH_3)_4Ru(py)$}$_2$($\mu$-dicyd)]$^{4+}$ complexes of this study. Because the Ru(III) ion is a poor $\pi$-donor of electron density,[4a] the mechanism for superexchange is most reasonably attributed to hole transfer via the HOMO of the bridging dicyd$^{2-}$ ligand. For the mixed-valence *trans*-[{$(NH_3)_4Ru(py)$}$_2$($\mu$-dicyd)]$^{3+}$ complexes, the trend in $\Delta G_r$ with bridging ligand can only be rationalized in terms of hole transfer superexchange. The magnitude of metal−metal coupling in these complexes proved too great to be

(37) Creutz, C.; Newton, M. D.; Sutin, N. *J. Photochem. Photobiol., A: Chem.* **1994**, *82*, 47.

(38) It should be noted that eq 6 differs from the corresponding equation in ref 37. We are grateful to Norman Sutin for pointing out to us that eq 6 is the correct form.

(39) It is not appropriate to quantitatively compare the value of $\epsilon$ to $\Delta G_r$ because of the interdependence of $\epsilon$ and $\lambda$.

treatable by the Hush model. However, the recently developed CNS model was extremely successful and gave a linear correlation between calculated and experimental estimates of metal−metal coupling. We are currently preparing complexes to test the CNS model in the strong coupling limit (a fully delocalized mixed-valence complex). The intervalence band properties could be modeled by PKS theory, provided that both vibronic and electronic factors were considered. The trend in the electronic coupling parameter $\epsilon$ followed the trend in metal−metal coupling. Finally, the magnitude of metal−metal coupling via Ru−dicyd−Ru linkages can be "tuned" by changing the electron donor properties of the spectator ligands, and this permits the purposeful design of molecular devices based on these linkages.

**Acknowledgment.** We are grateful to the Natural Sciences and Engineering Research Council of Canada for financial support (R.J.C., J.E.G., C.R). A.R.R. thanks the Islamic Republic of Iran for a graduate student scholarship. We also thank Johnson-Matthey P.L.C. for the loan of ruthenium trichloride hydrate.

**Supporting Information Available:** Full listings of crystal structure data, a labeled ORTEP diagram, a stereoview of the unit cell, tables of atomic parameters, anisotropic thermal parameters, bond lengths, and bond angles, and a figure showing the molar magnetic susceptibility from 5 to 300 K of $[\{(NH_3)_5Ru\}_2(\mu\text{-dicyd})][PF_6]_4$ (14 pages). Ordering information is given on any current masthead page.

IC9700260